

AD-A128 995

DEFORMATION AND FRACTURE AT ISOLATED HOLES IN
PLANE-STRAIN TENSION(U) MICHIGAN TECHNOLOGICAL UNIV
HOUGHTON DEPT OF METALLURGICAL EN..
R J BOURCIER ET AL. APR 83 TR-21

1/1

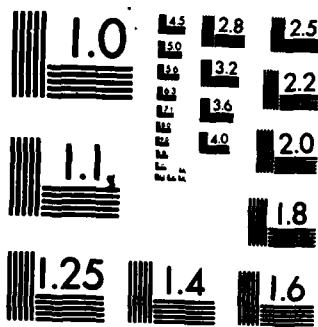
UNCLASSIFIED

F/G 20/11

NL



END
DATE
FILMED
OPTIC



MICROCOPY RESOLUTION TEST CHART
NATIONAL BUREAU OF STANDARDS-1963-A

12

TECHNICAL REPORT No. 21

TO

THE OFFICE OF NAVAL RESEARCH
CONTRACT No. N00014-76-C-0037, NR 031-756

DA 128995

DEFORMATION AND FRACTURE AT ISOLATED HOLES
IN PLANE-STRAIN TENSION

R. J. BOURCIER,[†] R. E. SMELSER,*
O. RICHMOND,* AND D. A. KOSS[†]

[†]DEPARTMENT OF METALLURGICAL ENGINEERING
MICHIGAN TECHNOLOGICAL UNIVERSITY
HOUGHTON, MI

*RESEARCH LABORATORY
U.S. STEEL CORPORATION
MONROEVILLE, PA

MP FILE COPY

DTIC
ELECTE
S JUN 8 1983
D

REPRODUCTION IN WHOLE OR IN PART IS PERMITTED FOR ANY
PURPOSE OF THE UNITED STATES GOVERNMENT. DISTRIBUTION
OF THIS DOCUMENT IS UNLIMITED.

88 06 06 05

REPORT DOCUMENTATION PAGE		READ INSTRUCTIONS BEFORE COMPLETING FORM
1. REPORT NUMBER No. 21	2. GOVT ACCESSION NO. A128 995	3. RECIPIENT'S CATALOG NUMBER
4. TITLE (and Subtitle) Deformation and Fracture at Isolated Holes in Plane-Strain Tension		5. TYPE OF REPORT & PERIOD COVERED
		6. PERFORMING ORG. REPORT NUMBER
7. AUTHOR(s) R. J. Bourcier, R. E. Smelser, O. Richmond, and D. A. Koss		8. CONTRACT OR GRANT NUMBER(s) N00014-76-C-0037, NR 031-756
9. PERFORMING ORGANIZATION NAME AND ADDRESS Dept. of Met. Eng., Michigan Tech Univ., Houghton, MI 49931 and Research Lab., U.S. Steel Corp., Monroeville, PA 15146		10. PROGRAM ELEMENT, PROJECT, TASK AREA & WORK UNIT NUMBERS
11. CONTROLLING OFFICE NAME AND ADDRESS Office of Naval Research 800 N. Quincy Street Arlington, VA 22217		12. REPORT DATE April, 1983
		13. NUMBER OF PAGES 23
14. MONITORING AGENCY NAME & ADDRESS (if different from Controlling Office)		15. SECURITY CLASS. (of this report) Unclassified
		15a. DECLASSIFICATION/DOWNGRADING SCHEDULE
16. DISTRIBUTION STATEMENT (of this Report) Distribution of this document is unlimited.		
17. DISTRIBUTION STATEMENT (of the abstract entered in Block 20, if different from Report)		
18. SUPPLEMENTARY NOTES		
19. KEY WORDS (Continue on reverse side if necessary and identify by block number) Deformation, Fracture, Ductile Fracture Mechanism, Holes, Plane-Strain Tension, Titanium Alloy, HSLA Steel, Finite-Element Modeling		
20. ABSTRACT (Continue on reverse side if necessary and identify by block number) The tensile behavior of plane-strain specimens each having a central hole with axis in the zero-strain direction has been examined. The study is based on the contrasting behavior of two materials, one with a relatively high strain hardening rate (an HSLA steel) and the other with a low rate (Ti-6Al-4V). Deformation of the holes, associated necking of the ligaments, as well as the overall force-elongation response exhibits excellent agreement with predictions from a large-strain elastoplastic finite-element model. Failure of the high strain-hardening material occurs by ductile tearing (cont d)		

20. Abstract (cont'd)

across the ligaments whereas failure of the low-hardening material occurs by shear localization. This is consistent with the predicted incremental plastic strain distributions as calculated by the finite element method. The experimental results and predictions of the finite-element models indicate the importance of work hardening in diffusing plastic flow in the presence of a geometric inhomogeneity

Accession For	
NTIS GRA&I	<input checked="" type="checkbox"/>
DTIC TAB	<input type="checkbox"/>
Unannounced	<input type="checkbox"/>
Justification	
By _____	
Distribution/	
Availability Codes	
Dist	Avail and/or Special
A	



DEFORMATION AND FRACTURE ~~AT~~ ISOLATED HOLES
IN PLANE-STRAIN TENSION

By: R. J. Bourcier*
R. E. Smelser**
O. Richmond**
D. A. Koss*

Abstract

The tensile behavior of plane-strain specimens each having a central hole with axis in the zero-strain direction has been examined. The study is based on the contrasting behavior of two materials, one with a relatively high strain hardening rate (an HSLA steel) and the other with a low rate (Ti-6Al-4V). Deformation of the holes, associated necking of the ligaments, as well as the overall force-elongation response exhibit excellent agreement with predictions from a large-strain elastoplastic finite-element model. Failure of the high strain-hardening material occurs by ductile tearing across the ligaments, whereas failure of the low-hardening material occurs by shear localization. This is consistent with the predicted incremental plastic strain distributions as calculated by the finite element method. The experimental results and predictions of the finite-element models indicate the importance of work hardening in diffusing plastic flow in the presence of a geometric inhomogeneity.

*Michigan Technological University, Department of Metallurgical Engineering,
Houghton, MI 49931

**U.S. Steel Corporation, Research Laboratory, Monroeville, PA 15146.

Introduction

Ductile fracture in high-strength alloys is a result of the termination of stable plastic flow by catastrophic strain localization. Microstructurally, this flow localization can often be traced to the presence of large voids within the material. These voids may be formed at large inclusions during straining or may already exist as porosity in a powder-metallurgy product or a casting. Within the highly strained regions joining these larger cavities, small voids can form at precipitates or small inclusions. These voids subsequently grow and coalesce to form the dimpled fracture surfaces characteristic of tensile failure in most ductile metals.

A large body of work has been performed in recent years in an attempt to identify the mechanical and microstructural variables that determine the deformation and fracture behavior of a material containing voids. Analytical studies [1-9], numerical work [10-13], and experimental investigations [14-17] have helped to characterize the qualitative influence of such factors as void fraction, hydrostatic stress, and work-hardening rate on both void growth and flow localization. However, while most of the theoretical work has modeled voids as holes in a two dimensional array, no study has yet been performed in which the flow and fracture behavior near an individual hole is examined both experimentally and analytically. In the present study, the deformation and fracture of a single-hole plane-strain tension specimen has been examined experimentally and analyzed by a large-strain elastoplastic finite-element model. Load-elongation and hole-growth behavior have been determined for two high-strength alloys with widely different mechanical responses. Good agreement is found between experiment and theory up to the point of flow localization in both cases. In addition, the predictions of the finite-element method (FEM) provided an insight into the detailed nature of the deformation history that results in the observed fracture behavior.

Experimental Materials and Procedures

To study the influence of mechanical-deformation parameters, two alloys were chosen: USS EX-TEN F50 Mod, a vanadium-strengthened, high-strength/low alloy (HSLA) steel, and Ti-6Al-4V, an alpha beta titanium alloy. The HSLA steel was chosen to represent a low-yield-strength, high-work-hardening material and the Ti-6Al-4V is typical of high-yield-strength, low-work-hardening alloys.

Single-hole plane-strain tension specimens, Figure 1, were prepared from both materials. The specimen geometry was chosen to provide a rigorous test of the FEM in a situation resembling the geometric features present in a material containing voids. The tensile direction was taken to be parallel to the rolling direction of the original plate. Load-extension curves were generated from specimens tested in uniaxial tension on a 10,000-kg Instron machine at an extension rate of 8.5×10^{-4} mm/s. Samples were strained to various levels (including failure), subsequently sectioned, and hole growth was measured as a function of total extension.

To provide stress-strain data as input for the FEM portion of the study, incremental plane-strain compression tests were performed on a 100,000 kg Baldwin hydraulic test machine. This mode of deformation was chosen to obtain accurate experimental flow data over the widest possible strain range. Tests performed on plane-strain tension specimens showed only very small strength-differential (S-D) effects [18,19] over the tensile-strain range for either material, and thus no attempt was made to calculate "tensile equivalent" flow curves. Compression tests were carried out at a cross-head speed of 3×10^{-3} mm/s on 4.2 mm thick plate specimens with the long transverse direction of the plate aligned in the direction of zero extension. Molybdenum disulfide and 0.076 mm thick teflon sheet were used as lubricants.

The experimental stress-strain data thus obtained were smoothed by means of analytic curve fitting by using a least-squares fit to the Swift equation,

$$\bar{\sigma} = \kappa(\bar{\epsilon}_p + \epsilon_0)^n, \quad (1)$$

where $\bar{\sigma}$ and $\bar{\epsilon}_p$ are the equivalent stress and plastic strain and κ , ϵ_0 , and n are constants. The resulting plane-strain compression flow curves for the HSLA steel and the Ti-6Al-4V are shown in Figure 2. The yield strength of the titanium alloy is approximately three times that of the HSLA steel (827 and 281 MPa, respectively), whereas the work-hardening rate is roughly one-third as large (0.063 vs. 0.176). The plastic-flow parameters calculated from these tests and the approximate elastic constants obtained from the literature [20] used in the FEM are summarized in Table I.

Finite-Element-Modeling Procedure

A finite-element model of the gauge section of the test specimen, Figure 1, has been constructed. Because of the symmetry of the specimen, it was only necessary to analyze one-quarter of the section. The initial finite-element mesh is shown in Figure 3. The boundary conditions imposed on the model are also shown. The exact boundary conditions imposed by the grips on the upper end of the gauge section are unknown. To bound the actual solution, two analyses for both materials were performed. One employed rigid grips, such that the transverse displacement $U_x = 0$, and the other a zero transverse traction, $T_x = 0$. The plastic-flow properties of the material were modeled by Equation (1). The FEM analysis was carried out with the large-strain elasto-plastic program FIPDEF [21-23] for isotropic work-hardening materials.

Results

Figures 4 and 5 show the results of the single-hole plane-strain tension tests. Differences in the shape and level of the experimental load-elongation curves, Figure 4, are consistent with the observed variations in flow parameters for these two materials. As is seen, the experimental and calculated load-extension curves exhibit quite good agreement for both materials up to and

even beyond the point of maximum load. The small overprediction of load may be due to several factors: small deviations from plane strain in the test specimens, neglect of the S-D effect, or the basic construction of the FEM mesh [24].

Hole growth in both materials, Figure 5, proceeds initially by axial extension. Transverse extension occurs at later stages of deformation. The hole-growth data in Figure 5 are not precisely comparable for experiment and analysis. The experimental hole-growth data were obtained by sectioning deformed specimens. Thus the amount of growth and extension represent plastic deformation only. In contrast, the numerical results include the elastic deformations. However, an estimate of the elastic recovery is on the order of a few tenths of a percent and would not influence the overall qualitative agreement. In addition, Figure 6 shows a comparison of the deformed mesh and specimen for the HSLA steel at a comparable stage of hole growth. The agreement in deformed shapes and necks lend support to the qualitative and quantitative predictive capabilities of the numerical simulation.

The differences between experiment and theory increase after the maximum load is attained. This is a consequence of both materials initiating their respective failure processes at strains near maximum load. In the titanium specimens, failure occurs catastrophically at maximum load by the development of a shear instability. The resulting fracture profile is one of mating inclined surfaces, Figure 7. In contrast, failure in the HSLA steel specimen occurs by the initiation of tearing on the transverse surfaces of the hole at a strain roughly corresponding to maximum load. These tears subsequently propagate to failure, resulting in a double-cup fracture profile, Figure 8.

As has already been noted, the FEM used here is not capable of accurately predicting the post-maximum-load deformation of either test material. The numerical results do, however, yield valuable information on the observed

failure mechanisms that result from the strain-hardening capacity of the test materials. The plastic shear strains near fracture for both the HSLA steel and the titanium alloy, although varying in magnitude, are qualitatively very similar. Both materials show the development of a band of maximum strain which links the hole with the outer free surface of the sample at roughly 45 degrees to the tensile axis. Given the large differences in mechanical response of these alloys, it would seem that this strain localization is primarily a result of the geometric discontinuity introduced into the sample by the hole.

On the basis of these data alone, both materials might be expected to fail by means of shear localization, giving fracture surfaces similar to those that are, in fact, observed experimentally only in the titanium. The distinction between the two alloys becomes more clear when the incremental plastic flow near failure is analyzed. Figures 7 and 8 show plots of incremental octahedral plastic strain for a nominal increment of extension of 0.033 percent. Deformation of the titanium alloy (Fig. 7) continues by the further development of the inclined deformation band due to the lack of sufficient work hardening to diffuse the plastic zone. Thus we expect that the eventual fracture of the specimen will result from shear localization and void linkup within this band, as is observed experimentally in Figure 7.

The incremental deformation of the HSLA steel, on the other hand, is in marked contrast to its accumulated strain distribution. As shown in Fig. 8, much of the incremental strain is distributed along the transverse ligament near the hole. This suggests that the EX-TEN F50 Mod material has sufficient work hardening to resist the early formation of an inclined deformation band encouraged by the test specimen. Given the fact that this material contains a relatively large number of inclusions and pearlite colonies from which voids can be nucleated, it might be expected that the calculated plastic strain gradients could result in the observed tensile rupture of the transverse

ligament by void nucleation, growth, and coalescence initiating at the hole surface.

Discussion and Conclusions

The results presented here illustrate the influence of work hardening on the development of plastic flow in the presence of a geometric inhomogeneity. In the Ti-6Al-4V material, the low rate of work hardening leaves the material with relatively little resistance to the rapid development of inclined bands of intense deformation from the hole surface outward to the specimen face. At a critical level of extension this ligament becomes plastically unstable, and fracture proceeds by shear localization and ductile rupture. In the HSLA steel, the high rate of work hardening allows deformation to be diffused; this prevents the development of the inclined deformation band due to shear localization. As a result, considerable hole growth occurs, much tensile elongation takes place in the ligament, and failure occurs via tensile rupture.

It seems likely that the processes seen here should be analogous to those operative in the fracture of materials containing voids or porosity. Although the deformation zones induced by a random array of voids/pores will be different in detail from those in our simple model, the principal effect will still be one of geometrically-induced flow localization. The ability of the matrix material to distribute strain within the ligaments between the voids/pores is critical in determining the rate at which this localization proceeds. For a given void population, increased work hardening will delay the onset of instability. However, the delay is achieved at the expense of considerable tensile deformation within the ligaments and resulting hole growth. Given the presence of second phase particles or small inclusions which may deband or fracture at small strains, the ligaments may fail by a ductile tearing mode normal to the tensile axis in a material with a high work hardening capacity.

In conclusion, this study demonstrates the influence of work hardening on material deformation and failure in the presence of a geometric inhomogeneity. Agreement between experiment and continuum plasticity theory FEM is very good for straining prior to the development of plastic flow localization. Additionally, the predicted character of the developing plastic zone at the onset of fracture suggests how the failure process proceeds. In particular, the work hardening rate is viewed as critical in determining whether failure occurs by: (1) a shear localization process when the strain hardening rate is low (Ti-6Al-4V) or (2) a tensile rupture process which is associated with considerable hole growth and a high rate of work hardening (the HSLA steel). These results suggest that a similar approach might be applicable to the analysis of deformation and fracture in high-strength materials containing large-scale pre-existing porosity.

Acknowledgement

The authors are grateful to R. J. Sober and W. A. Spitzig for their assistance with specimen preparation and testing and to the Office of Naval Research, who supported the work under Contract No. N00014-76-C-0037, NR 031-756.

REFERENCES

1. F. A. McClintock, S. M. Kaplan, and C. A. Berg, *International Journal of Fracture Mechanics*, 2 (1966) 614-627.
2. F. A. McClintock, *Journal of Applied Mechanics*, 35 (1968) 363-371.
3. P. F. Thomason, *Journal of the Institute of Metals*, 96 (1968) 360-365.
4. J. R. Rice and D. M. Tracey, *Journal of the Mechanics and Physics of Solids*, 17 (1969) 201-217.
5. D. M. Tracey, *Engineering Fracture Mechanics*, 3 (1971) 301-315.
6. A. L. Gurson, in *Fracture 1977*, Vol. 2, University of Waterloo Press, Waterloo (1977) 357-364.
7. H. Yamamoto, *International Journal of Fracture*, 14 (1978) 347-365.
8. A. Melander and U. Stahlberg, *International Journal of Fracture*, 16 (1980) 431-440.
9. P. F. Thomason, *Acta Met.*, 29 (1981) 763-777.
10. S. N. Shah, S. Kobayashi, and S. I. Oh, "Theories of Flow and Fracture in Metalworking Processing, Parts I and II," AFML-TR-76-61 (AS-A0127 266/6GA), Dept. of Mechanical Engineering, Univ. of California at Berkeley (1976).
11. A. Needleman, *Journal of Applied Mechanics*, 35 (1972) 964-970.
12. S. Nemat-Nasser and M. Taya, *International Journal of Solids and Structures*, 16 (1980) 483-494.
13. V. Tvergaard, *International Journal of Fracture*, 17 (1981) 389-408.
14. B. I. Edelson, *Trans. ASM*, 56 (1963) 82-89.
15. J. Gurland and J. Plateau, *Trans. ASM*, 56 (1963) 442-454.
16. M. Perra and I. Finnie, in *Fracture 1977*, Vol. 2, Univ. of Waterloo Press, Waterloo (1977) 415-423.
17. R. J. Bourcier and D. A. Koss, in *Advances in Fracture Research*, Vol. I, Pergamon Press, London (1982) 187-194.
18. W. A. Spitzig, R. J. Sober, and O. Richmond, *Acta Met.*, 23 (1975) 885-893.
19. W. A. Spitzig, R. J. Sober, and O. Richmond, *Met. Trans.* 7A (1976) 1703-1710.
20. *Metals Handbook*, Ninth Edition, Vols. 1 and 2, American Society for Metals, Metals Park (1979).
21. J. R. Osias and J. L. Swedlow, *International Journal of Solids and Structures*, 10 (1974) 321-339.

22. E. J. Appleby, M. L. Devenpeck, L. M. O'Hara, and O. Richmond, in Applications of Numerical Methods to Forming Processes, American Society of Mechanical Engineers, New York, (1978) 95-105.
23. C. Y. Lu, E. J. Appleby, R. S. Rao, M. L. Devenpeck, P. W. Wright, and O. Richmond, to appear in Proceedings of the International Conference on Numerical Methods in Industrial Forming Processes, Swansea, United Kingdom (1982).
24. J. C. Nagtegaal, D. M. Parks, and J. R. Rice, Computer Methods in Applied Mechanics and Engineering, 4 (1974) 153-177.

TABLE I

The Mechanical Parameters Used in the Finite-Element Modeling

	<u>Ti-6Al-4V</u>	<u>EX-TEN F50-Med</u>
E (Youngs Modulus) MPa	110 x 10 ³	193 x 10 ³
v (Poissons Ratio)	0.33	0.29
K, MPa	1170	789
Eo	0.0039	0.0029
n	0.0626	0.1764

Figures

- Fig. 1. The single-hole plane-strain tension specimen; the dimensions are in mm.
- Fig. 2. Stress-plastic strain curves for Ti-6Al-4V and the HSLA steel, EX-TEN F50 Mod.
- Fig. 3. FEM mesh for modeling single-hole plane-strain tension specimen. U_i and T_i denote displacement and traction components, respectively.
- Fig. 4. Load-elongation curves for single-hole plane-strain tension specimens.
- Fig. 5. Hole growth for (a) Ti-6Al-4V, and (b) the HSLA steel, EX-TEN F50 Mod.
- Fig. 6. Comparison of single-hole plane-strain tension specimen and finite-element model at equivalent axial hole growth, $y/y_0 = 1.31$.
- Fig. 7. A fracture profile and contours of incremental octahedral plastic strain for Ti-6Al-4V. The increment of extension is 0.033% and occurs near fracture.
- Fig. 8. A fracture profile and contours of incremental octahedral plastic strain for the HSLA steel, EX-TEN F50 Mod. The increment of extension is 0.033% and occurs near fracture.

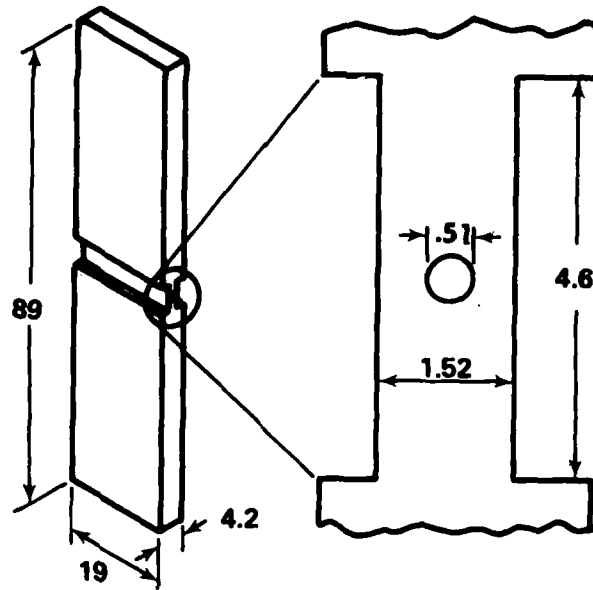


Fig. 1. The single-hole plane-strain tension specimen; the dimensions are in mm.

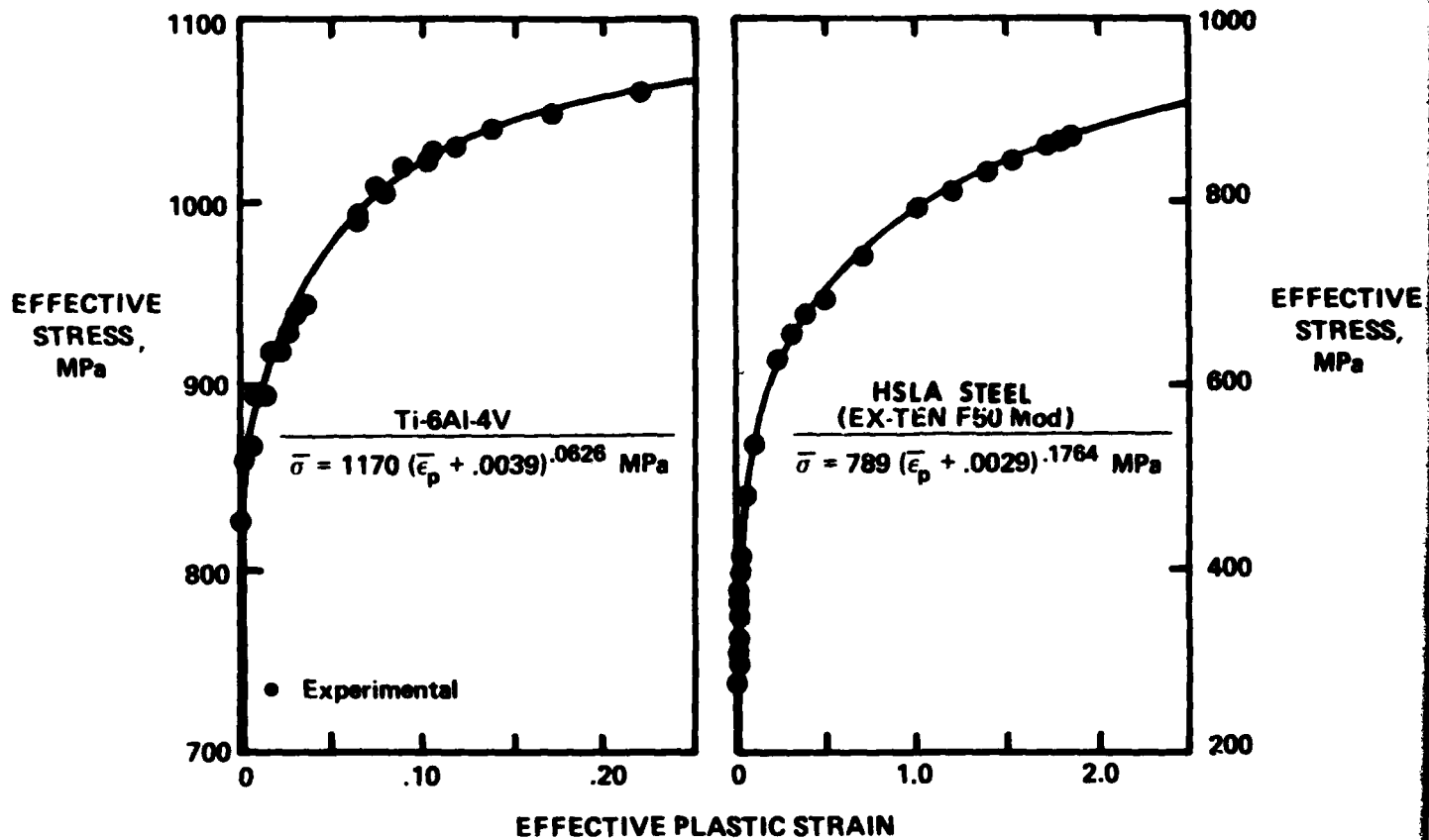


Fig. 2. Stress-plastic strain curves for Ti-6Al-4V and the HSLA steel, EX-TEN F50 Mod.

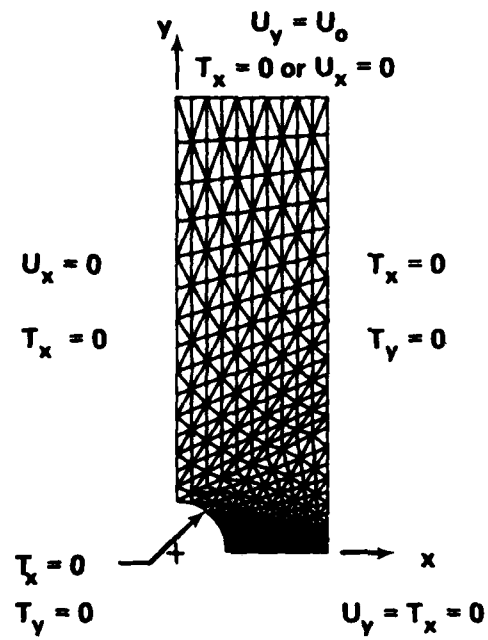


Fig. 3. FEM mesh for modeling single-hole plane-strain tension specimen. U_i and T_i denote displacement and traction components, respectively.

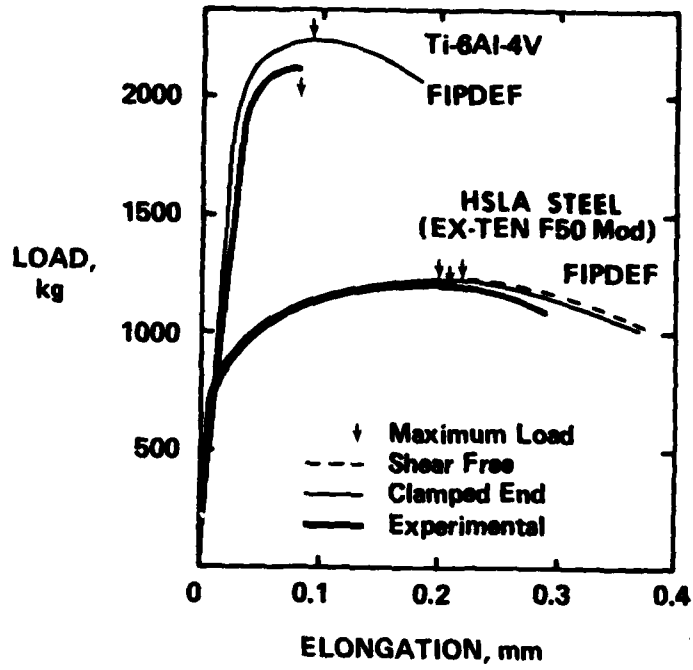


Fig. 4. Load-elongation curves for single-hole plane-strain tension specimens.

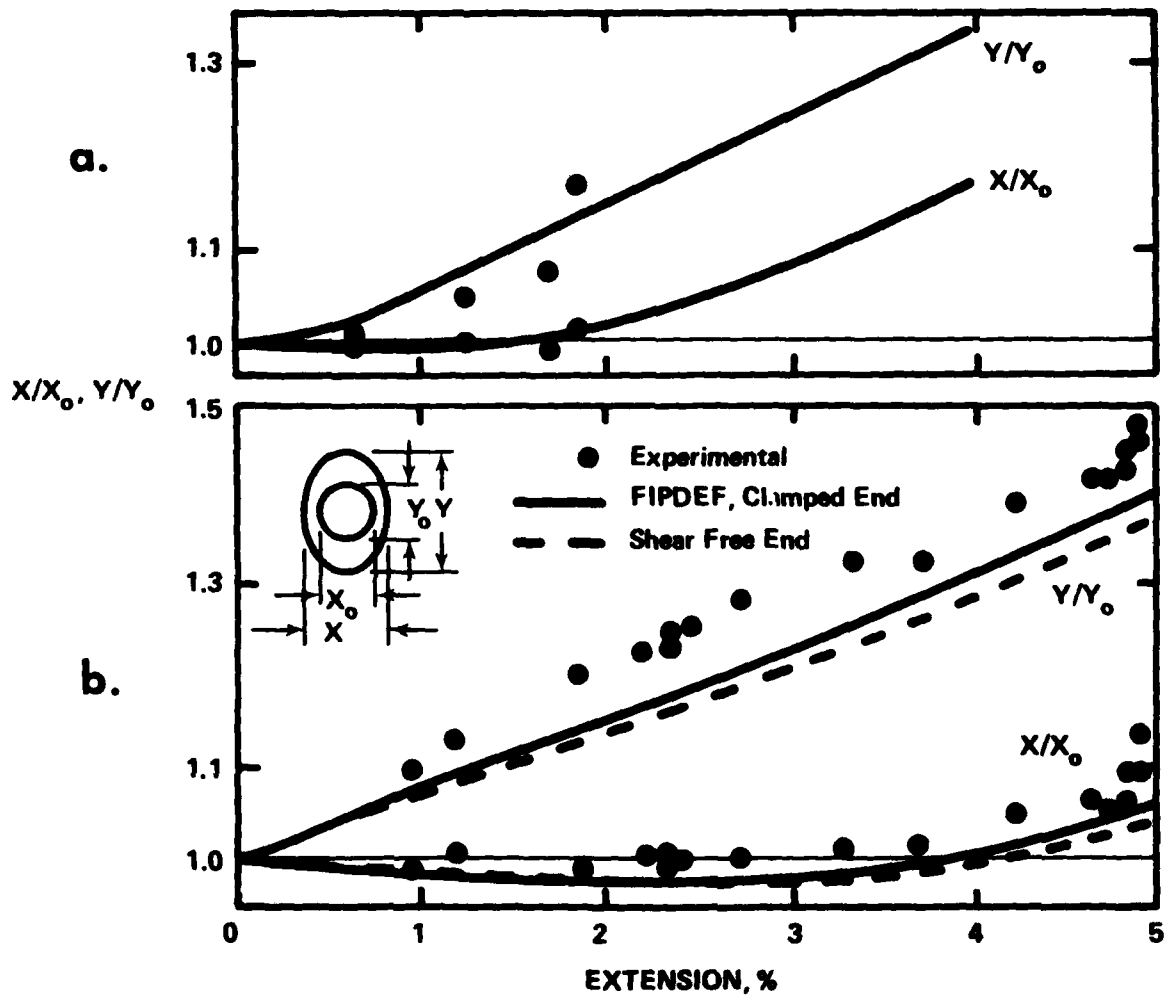


Fig. 5. Hole growth for (a) Ti-6Al-4V, and (b) the HSLA steel, EX-TEN F50 Mod.

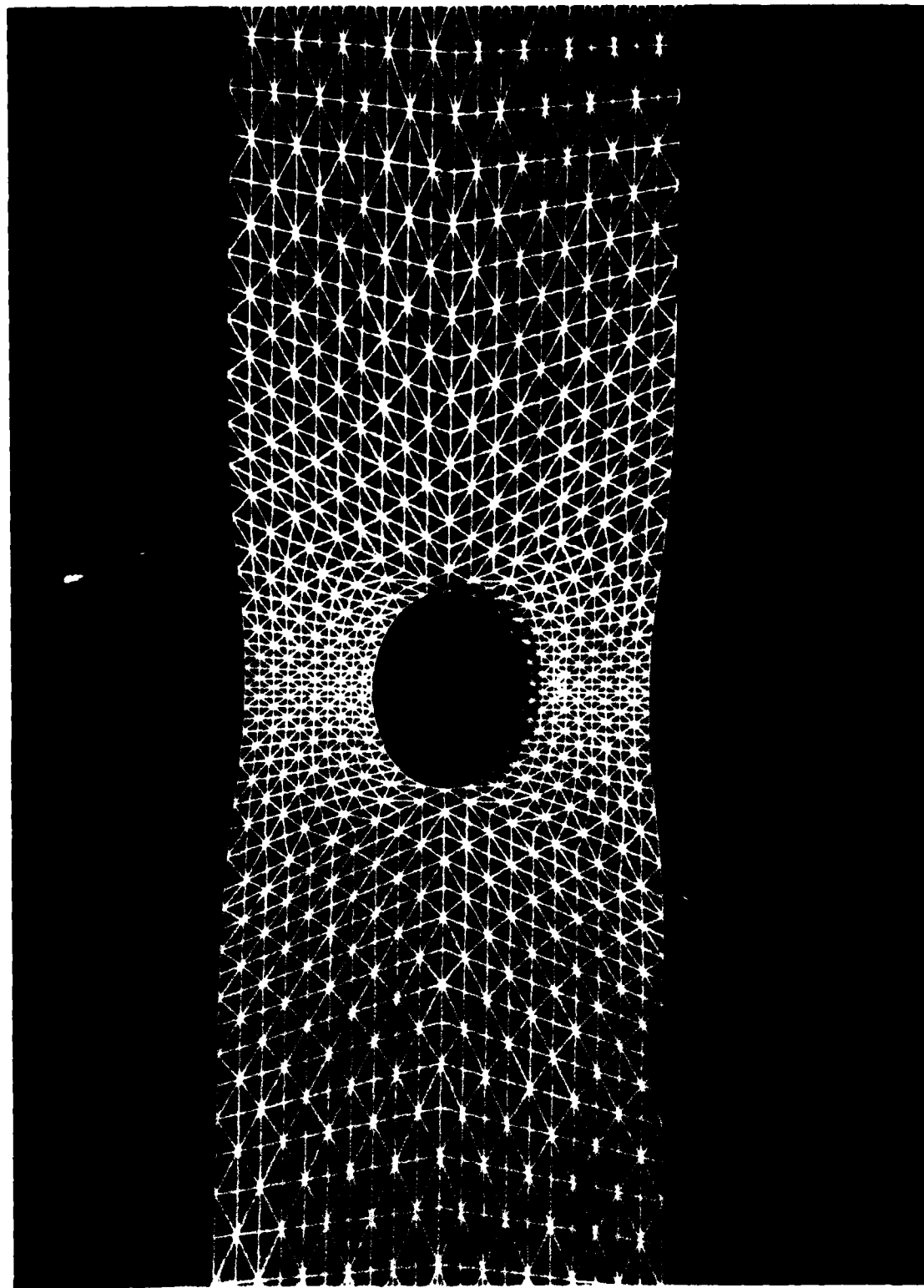


Fig. 6. Comparison of single-hole plane-strain tension specimen and finite-element model at equivalent axial hole growth, $y/y_0 = 1.31$.

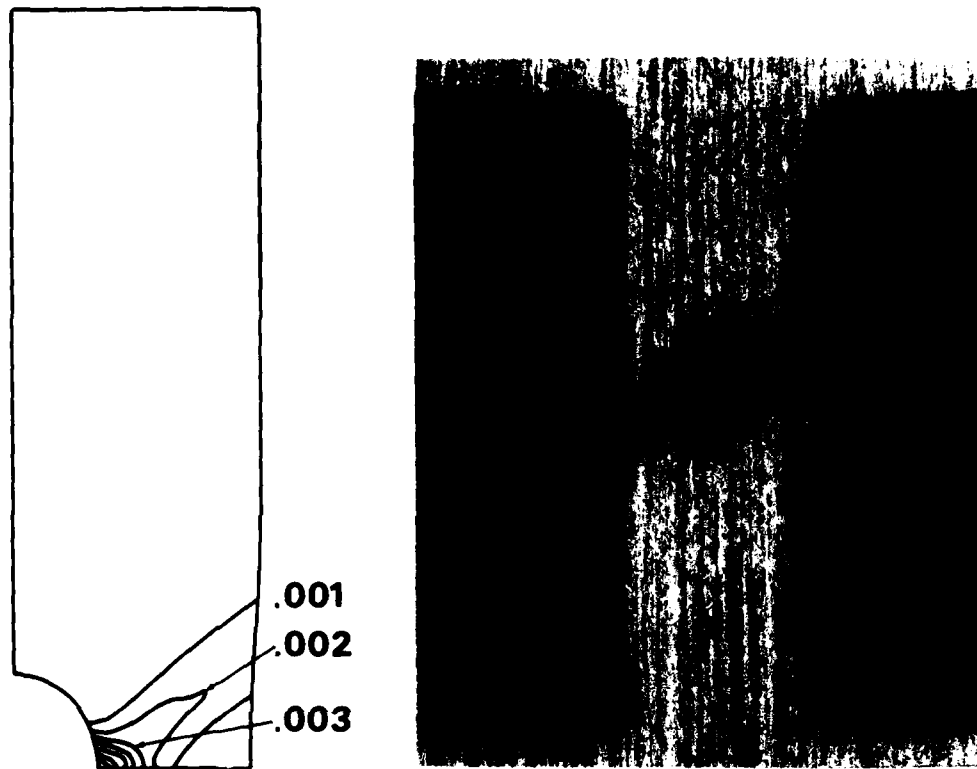


Fig. 7. A fracture profile and contours of incremental octahedral plastic strain for Ti-6Al-4V. The increment of extension is 0.033% and occurs near fracture.

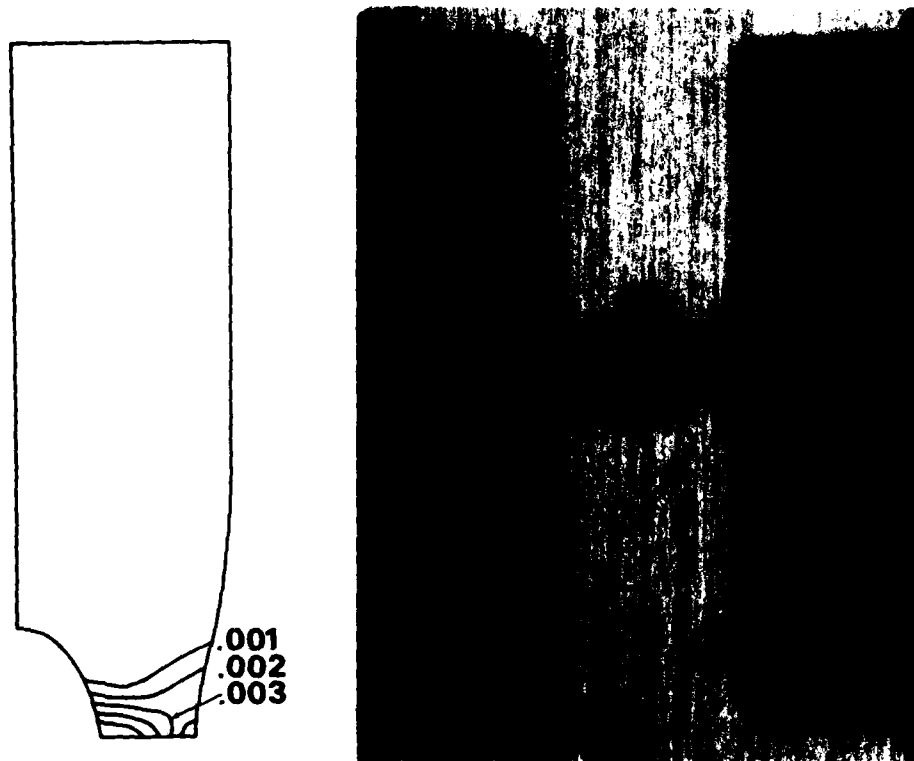


Fig. 8. A fracture profile and contours of incremental octahedral plastic strain for the HSLA steel, EX-TEN F50 Mod. The increment of extension is 0.033% and occurs near fracture.